Studies of Ultracold Hydrogen

Principal Investigators

Prof. Daniel Kleppner and Prof. Thomas J. Greytak

Project staff

David Landhuis, Stephen C. Moss, Walter Joffrain, Lia Matos, Margaret Pan, Julia K. Steinberger, Kendra Vant, Dr. Lorenz Willmann

Sponsors

National Science Foundation, Office of Naval Research

1 Introduction

Trapped ultracold hydrogen provides a unique laboratory for exploring many areas of atomic physics. We are currently carrying out research in Bose-Einstein condensation (BEC), collisional physics of metastable atoms, precision measurements of hydrogen transition frequencies, and sympathetic trapping and cooling of deuterium.

2 Experimental Methods

Trapping and Cooling

Our experiments are based on trapping of atomic hydrogen in a cryogenic apparatus (Fig. 1) [1]. Molecular hydrogen is dissociated in an rf resonator thermally anchored to the mixing chamber of a dilution refrigerator. The resulting hydrogen atoms are cooled by interaction with the walls of a trapping cell so that the $1S$ $|F = 1, m_F = 1\rangle$ hyperfine state is trapped in a 0.5 K deep Ioffe-Pritchard magnetic trap [2]. The trap fields are generated by superconducting magnets. Atoms with sufficient energy can evaporate over a magnetic saddlepoint at one end of the cylindrical trap. By progressively lowering the field of the saddlepoint, evaporative cooling is forced. In this way, the sample can be cooled from an initial temperature of approximately 40 mK to around 200 μK.

The temperature can be reduced another order of magnitude by rf evaporation (see Sec. 3) using coils wrapped on the inside of a non-conducting section of the refrigerator vacuum chamber. For typical atom densities in our trap, BEC is achieved at around 50 μK, and we have generated samples as cold as 20 μK. For some BEC experiments, we find it useful to make two separate sweeps of the rf frequency. The first sweep reduces the temperature to just above the BEC transition; the second sweep makes a rapid "rf cut" through the thermal cloud, initiating condensate formation in a controlled manner.

Cooling comes at the expense of atom number. As the trap cycle proceeds atoms are lost both due to evaporation and to inelastic collisions which cause transitions to untrapped magnetic states. Initially, more than 10^{14} atoms are loaded into the trap. A few times 10^{10} atoms remain when the degenerate regime is reached. Nevertheless, the peak atom density increases from 10^{13} cm^{-3} after loading to a few times 10^{14} cm^{-3} at the BEC transition. This is because the volume occupied by the atom cloud decreases dramatically as the sample cools.

1S-2S Spectroscopy

Our primary tool for probing the atoms is excitation spectroscopy of the two-photon $1S$-$2S$ transition with a 243 nm UV laser [3, 4, 2]. To generate the UV, we double the frequency of a 486 nm dye laser which has been stabilized to about 1 kHz. In a typical spectroscopic measurement, laser pulses of $1 \sim 4$ ms duration

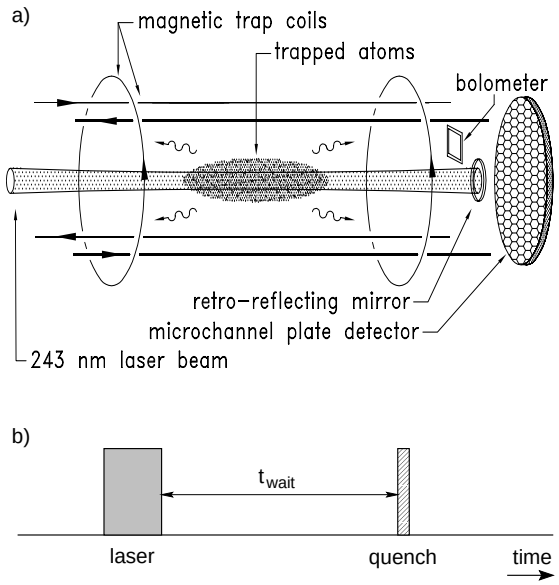

Figure 1: (a) A schematic of the cryogenic trapping apparatus. The atoms are trapped at the minimum of the Ioffe-Pritchard field. The excitation laser, which is focused to a 25 μm radius, is reflected back on itself to permit Doppler-free two-photon excitation. The atoms and retro-mirror are inside a G-10 trapping cell (not shown here). (b) Timing diagram for $1S$-$2S$ excitation spectroscopy. At a time $t_{\rm wait}$ after excitation, the metastables are Stark-quenched by an electric field pulse, resulting in a burst of Lyman-α photons.

excite a small fraction of the ground state atoms to the metastable $2S$ state. After a wait time of $1 \sim 90$ ms, the metastable atoms are Stark-quenched by an applied electric field of approximately 10 V/cm; in a few microseconds the excited atoms relax back to the ground state, emitting Lyman-α photons which are counted on a microchannel plate detector (MCP). The separation of excitation and detection pulses and the ability to quench the metastables all at once help to minimize the background, mostly laser-induced fluorescence from different parts of the trapping cell. In a typical spectroscopic measurement, the 243 nm laser frequency is stepped back and forth across a portion of the $1S$-$2S$ spectrum, with one or more laser shots at each frequency step. The metastable decay behavior can be observed by cycling through a number of different wait times at each step.

The two-photon excitation spectrum consists of Doppler-free and Doppler-sensitive features, separated by a recoil shift [2]. The Doppler-free transition is very narrow, with linewidths in our experiment varying between a few kHz and several tens of kHz at 243 nm depending on the temperature and density of the sample. At higher temperatures, the linewidth is determined primarily by time of flight broadening, reflecting the finite time atoms spend in the laser beam. At lower temperatures and higher atom densities, the width of the Dopper-free line is dominated by the density-dependent cold collision shift [4]. The Doppler-sensitive line, which has a shape reflecting the velocity distribution of the sample, has roughly the same total intensity as the Doppler-free line but is much broader (several MHz); we are only able to resolve the Doppler-sensitive spectrum below about 200 μK. To observe metastable density effects, it is desirable to excite as many metastables as possible by tuning the laser near the Doppler-free resonance, where excitation rates are highest. When a condensate is present, there is an additional contribution to both the Doppler-free and Doppler-sensitive portions of the $1S$-$2S$ spectrum. In each case, the BEC feature lies to the red of the line center, and is spread over several hundred kilohertz due to the large densities present in the condensate.

The addition of a copper film to the inside of our non-conducting trapping cell has been an important enhancement to our current apparatus. The film is thin enough to allow rf power to reach the atoms from antennas outside, but thick enough to shield stray electric fields which previously limited the metastable lifetime to ~ 1 ms. We now routinely observe metastable lifetimes of 90 ms in our trap. In 2000, we increased

our signal rate by eliminating a Lyman-α filter in front of the MCP. To protect the detector from saturation by 243 nm laser scatter, a high-voltage switching circuit turns on the MCP gain only when detecting Lyman-α. For the case of the condensate spectrum, we further improved signal strength by reducing the laser beam radius by a factor of two, thereby increasing peak laser intensity by a factor of four. With all changes, the BEC signal rate is now an order of magnitude larger than in our initial experiments of 1998.

3 Condensate Growth in Atomic Hydrogen

The discovery of Bose-Einstein condensation (BEC) in trapped atomic gases has initiated an intense period of experimental and theoretical research. Much is now known about the equilibrium properties of these systems, but many non-equilibrium aspects remain to be understood. Among these is the non-equilibrium process of formation of a condensate from a trapped, non-degenerate gas of bosons. There have been many theoretical invesigations into the problem of condensate formation, but to date only one experimental study using Na has explored the problem [5], and there are some discrepancies to resolve. Recently our group has made detailed studies of the growth of a hydrogen BEC.

Trapped atomic hydrogen is an excellent system in which to study condensate growth. Compared to alkali atoms, the s-wave scattering length, a, is anomalously small. For example, $a_{Na}/a_H \sim 42$. Since the rate of thermalizing elastic collisions depends on a^2, cooling of a trapped hydrogen gas procedes slowly. As a result, the characteristic time to form a condensate is a few seconds rather than 100 ms.

For these reasons we have carried out experiments that provide a detailed, quantitative test for theories of condensate growth.

Experiment

RF Evaporation

A central technique for carrying out condensate growth experiments is evaporation using radio frequency (rf) spin resonance. To reach temperatures below 200 μK we apply an rf field that causes transitions to an untrapped magnetic sublevel wherever the trapping magnetic field satisfies the resonance condition. To perform forced evaporation and cool the trapped sample, we slowly reduce the frequency of the rf field. This has the effect of removing only the most energetic atoms from the trap while allowing the remaining atoms to redistribute energy. In this way the temperature of the sample is reduced. It is important to note that the rf frequency is reduced slowly so that the trapped atomic sample remains in thermal equilibrium.

RF-Cut Experiment

To study condensate growth, we use rf evaporation to cool the trapped sample to a temperature just above the critical temperature, T_c, at which the condensate will form. The rf frequency is then reduced swiftly and subsequently held constant in order to cut into the trapped sample. This "cut" produces a non-equilibrium distribution in the trap, unstable against condensate formation. We then monitor the re-establishment of equilibrium, and hence the formation of a condensate, using $1S$-$2S$ spectroscopy.

The slow cooling by rf evaporation and excellent reproducibility of our system allows us to produce a non-degenerate gas of trapped bosons with a well-known temperature and density. By varying the rate and depth of the rf cuts, we perform experiments that are well-characterized and suitable to quantitative comparison with theory. Figure 2 shows an example of two such cuts.

Comparison with Theory

Theories of condensate growth predict how the number of atoms in the condensate changes in time. To date none of these theories has included loss processes from the trapped sample. In alkali systems, the time scale for loss from the condensate is long compared to the growth time scale. For hydrogen, the situation is different. The primary loss mechanism for the condensate is dipolar spin relaxation. The characteristic condensate dipolar decay time is ~ 2 s, on the same order as the time for condensate formation. Thus, for quantitative

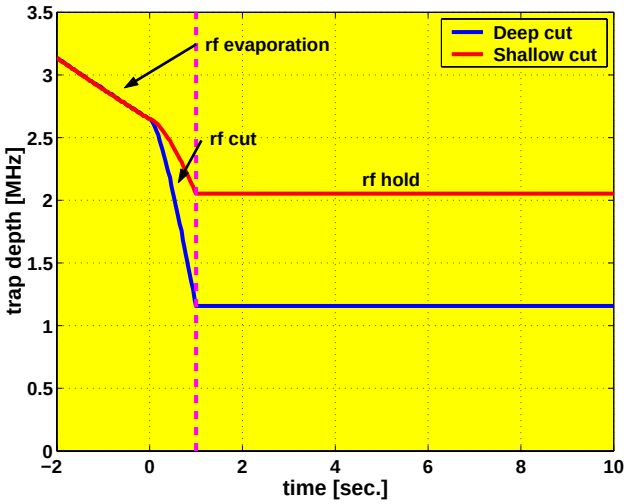

Figure 2: "RF-cut method": rf frequency as a function of time. The slow rf evaporation sweep is followed by a one second cut to various ending frequencies.

comparisons with theory, the theory must include loss processes. In collaboration with H. T. C. Stoof we have extended the theory of condensate growth [6] to include evaporation, a time dependent rf cut, and dipolar relaxation.

By itself $1S$-$2S$ spectroscopy does not provide a direct measure of condensate number versus time. Instead we monitor the spectroscopic lineshape due to the condensate as a function of time. The $1S$-$2S$ transition frequency is redshifted by an amount proportional to the density. The signal observed at a particular frequency is proportional to the number of condensate atoms at the corresponding density. Thus the appearance of a spectroscopic feature at large redshift indicates the presence of a condensate.

We assume that the condensate density is well-described by a Thomas-Fermi profile, $n(\rho, z) = n_p - V(\rho, z)/U$ where n_p is the peak density in the condensate, $V(\rho, z)$ is the magnetic trapping potential, and $U = 4\pi\hbar^2 a/m$ characterizes the strength of interactions between atoms. Under this assumption, it turns out that the number of condensate atoms, N_0, is related to the peak density by $N_0 = C n_p^{5/2}$, where C is a known factor characterizing the trap. Thus, by finding the peak redshift of the condensate lineshape we find the peak density and hence the condensate number. Put another way, by monitoring the peak redshift as a function of time, we monitor the condensate population as a function of time.

Figure 3 shows an example of the condensate spectra observed using Doppler sensitive excitation. The condensate lineshape is well described using a Thomas-Fermi density profile. The lineshape sits on top of the broad Doppler profile due to non-condensed atoms. By fitting the observed condensate spectra as a function of time, we extract the peak density and therefore the condensate number as a function of time. This allows us to make quantitative comparisons with our numerical model of condensate growth [7].

In Figure 4 we give an example of the comparison between our numerical model and experimental data. The model takes as input parameters initial atom number, N, and initial temperature, T. The single parameter that scales the experimental data is the $1S$-$2S$ scattering length, a_{1S-2S}. We find good agreement with the model for $a_{1S-2S} = -1.45$ nm. This is in excellent agreement with the value measured by Killian *et al.* [4] of $-1.4(0.3)$ nm.

In summary, we have made detailed experiments on the growth of a hydrogen condensate. A comparison of the data with our improved numerical model of condensate growth indicates that we have a good understanding of the non-equilibrium behavior of our trapped sample.

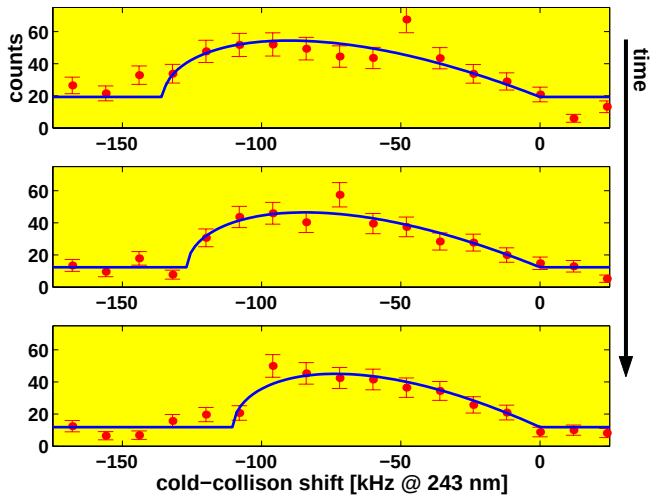

Figure 3: Fit of the condensate lineshape using a Thomas-Fermi density profile. Note that the peak shift is decreasing at later times indicating the decay of the condensate. By extracting the peak shift as a function of time, we determine the number of condensate atoms as a function of time.

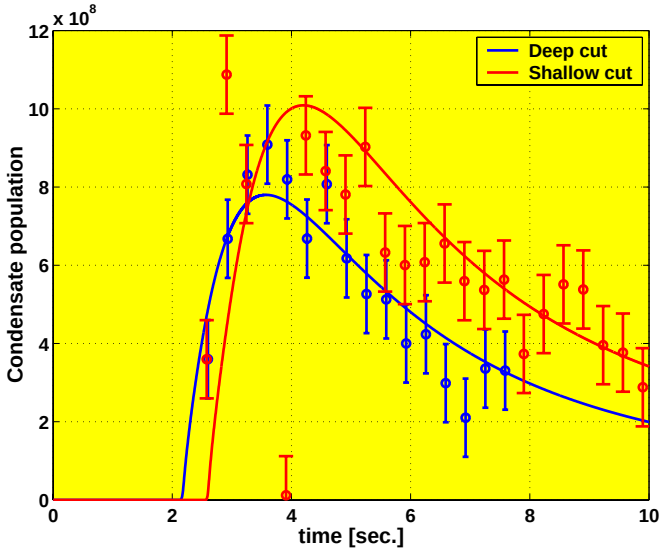

Figure 4: Comparison of numerical model describing condensate growth and decay and data taken after applying the rf cuts depicted in Figure 2. Initial conditions for the model are $N = 2.6 \times 10^{10}$ non-condensed atoms at $T = 50$ μK.

4 Trapped Metastable H

Motivation

Ultracold metastable hydrogen provides an excellent new medium for ultraprecise spectroscopy of hydrogen. Precision measurements of $2S$-nS transitions ($n > 2$) can be combined with the existing precise measurement of the $1S$-$2S$ frequency [8] to derive better values for the Rydberg constant and the $1S$ Lamb shift [9]. The best measurements of $2S$-nS frequencies to date have employed thermal atomic beams and high power lasers. The precision is limited by uncertainty in the AC Stark shift correction required for the intense laser field. In a cold, trapped sample of metastable H, the laser power requirements are greatly reduced, and the precision of $2S$-nS frequency measurements can be improved by an order of magnitude. This would lead to similar improvements in the Lamb shift and Rydberg constant.

As a first step toward precision $2S$-nS spectroscopy, we have demonstrated that we can produce clouds of $\sim 10^7$ metastables with lifetimes approaching 100 ms. (Similar lifetimes were achieved a few years ago in a stainless steel trapping cell [3]. However, the metal cell precluded use of rf evaporation, which makes accessible the high densities and low temperatures necessary for our large excitation rates.)

A second avenue of research involves the collisional physics of metastable H. In particular, we have performed decay measurements providing information about inelastic collisions in the ultracold regime. The $2S$-$2S$ inelastic collision channels which may be important in our trap include Penning ionization, associative ionization, and excitation transfer, in which $2S$ atoms are converted to $2P$ atoms [10]. This last process is also known as collisional quenching. Dipolar decay collisions between metastables, like those responsible for density decay of the ground state sample, are unlikely to play a role at the metastable densities in our experiment ($< 10^{11}$ cm^{-3}). Processes which are essentially one-body in nature also contribute to the population decay. Aside from the natural radiative decay, metastables can be quenched by stray electric fields or undergo inelastic collisions with $1S$ atoms.

Samples of cold metastable atoms are also interesting because they possess an internal energy which is enormous compared to their translational energy. This large internal energy, 10 eV in the case of H, is easily detected in a collision with a surface, making possible quantum optics experiments involving single-atom detection [11, 12]. In addition, a bright beam of cold metastables may be ideal for atom lithography [13].

Decay Measurements

Recently, we have observed a density-dependent decay behavior of the metastable cloud [14]. A decay measurement is made by exciting a cloud of metastables multiple times under constant conditions and quenching at different times after excitation. The number of Lyman-α fluorescence counts observed at each quench is taken to be proportional to the remaining metastable population. A decay curve of 8 time points is recorded in 800 ms, and hundreds of such measurements can be made in a single trap cycle. The data is corrected for background fluorescence using identical measurements made at the end of the trap cycle with the laser tuned off resonance.

To minimize the effect of stray electric fields, we apply a compensating DC field with the same electrodes used to quench the atoms (Fig. 5). The compensation voltage is determined at a relatively high temperature (2 mK), where the density of metastables is relatively low, and the decay appears consistent with a simple exponential (one-body loss). The typical minimum decay rate observed is ~ 11 s^{-1}, corresponding to a lifetime of 90 ms, about 3/4 of the 122 ms natural lifetime. In the present design, compensation of stray fields is possible only along one axis transverse to the trapping cell (Fig. 5a), and we attribute the shortened lifetime to residual stray fields of about 30 mV/cm. Inelastic collisions between metastables and ground state atoms could also contribute to the one-body loss. However, since similarly long lifetimes have been observed for a range of ground state densities, these processes are probably not significant.

The highest metastable densities, $\sim 10^{10}$ cm^{-3}, are achieved in the rf evaporation regime. If the decay curves are fit with single exponentials, we find decay rates as high as three times the natural decay rate (Fig. 6). By scanning back and forth across the $1S$-$2S$ resonance, and by scanning long enough for the $1S$ sample to decay, metastable decay curves are recorded for a range of initial metastable numbers. When the decay curves are binned together according to the signal strength immediately after excitation, it is clear

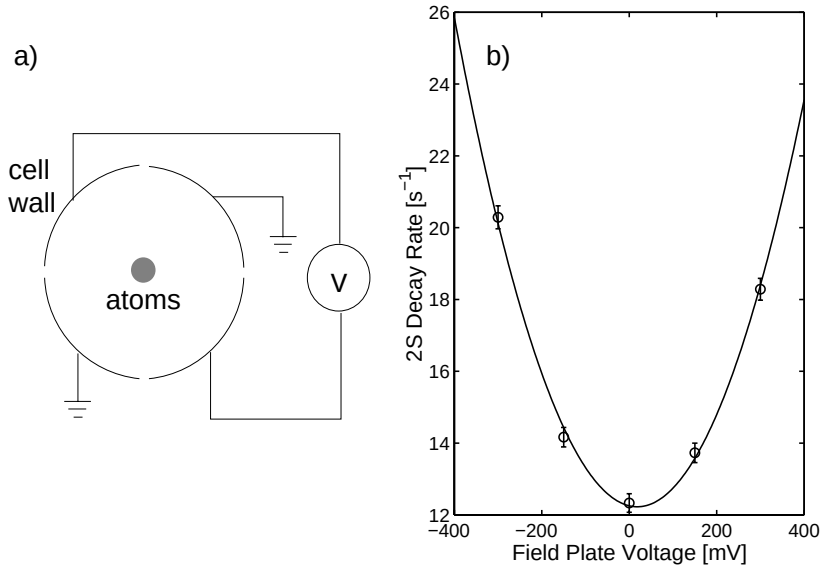

Figure 5: (a) Schematic showing cross section of trapping cell and electrical connections for the copper film electrodes used to apply both quenching electric field pulses and a small DC compensation field. (b) Example of decay rate measurements for different applied DC fields for a single trapped sample. A parabola is fit to the data points, indicating the quadratic dependence of Stark quenching rate on the applied electric field.

that the decay rate increases as $2S$ number increases, which also corresponds to an increase in metastable density.

When the $2S$ density is large, the decay is better described by a model which includes both one- and two-body decay. If the volume occupied by the metastables does not change much during the decay, the loss rate due to $2S$-$2S$ collisions will be proportional to the square of the metastable number. Thus, we postulate $N(t)$, the number of counts observed at a wait time t, to be a solution of $\dot{N} = -\alpha_1 N - \alpha_2 N^2$. Fig. 7 shows decay data from a 110 μK sample fitted with this "one-plus-two" model and with a simple exponential. If α_1 is fixed at the decay rate determined at low metastable density, the only remaining free parameters are α_2 and an amplitude factor. In this way, we can fit values for α_2 for different initial numbers of metastables excited at the same temperature. We find α_2 to be independent of initial number within uncertainties, confirming that the model is reasonable.

Two-Body Loss Rate

Given the metastable density immediately after the excitation pulse, the fit parameter α_2 can be used to determine a two-body loss rate constant K_2, defined by

$$\left.\frac{dn}{dt}\right|_{\text{two body}} = -K_2 n^2 \tag{1}$$

where n is the local metastable density. Under the assumptions that the relative spatial distribution of metastables is static and that $2S$-$2S$ inelastic collisions are the dominant loss channel,

$$K_2 = \epsilon G \alpha_2, \tag{2}$$

where G is a geometry factor dependent on the temperature, the magnetic trap shape, and the laser intensity distribution, and ϵ is the Lyman-α detection efficiency in our apparatus.

In reality, the metastable distribution is not static. This is because atoms are preferentially excited near the focus of the laser beam, where the laser intensity is highest. After excitation, the metastables diffuse

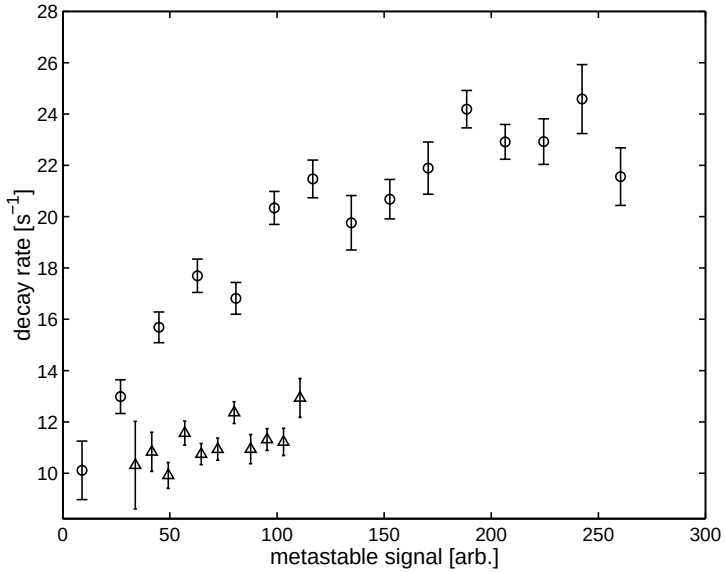

Figure 6: Decay rates as a function of metastable signal, determined from simple exponential fits for samples at 2 mK (triangles) and 110 μK (circles). The bottom of the graph corresponds to the natural decay rate of 8.2 s^{-1}. The initial ground state densities of the two samples are about 2×10^{13} and 1×10^{14}, respectively. For the same metastable signal, the metastable density at 2 mK is much smaller than at 110 μK due to a much larger effective volume for the metastable cloud.

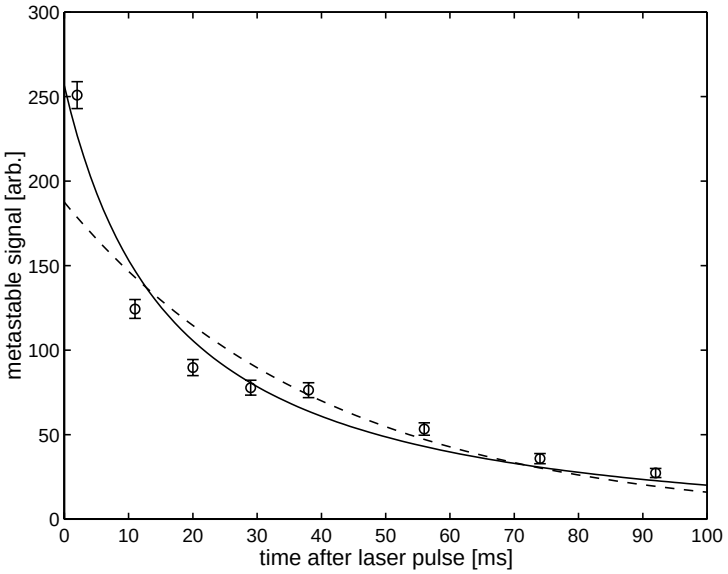

Figure 7: Example decay data for a 110 μK sample. The error bars include statistical errors only; additional scatter arises from fluctuations in the laser alignment. The fitted curves show that a model including two-body decay (solid) describes the decay better than a simple exponential (dashed).

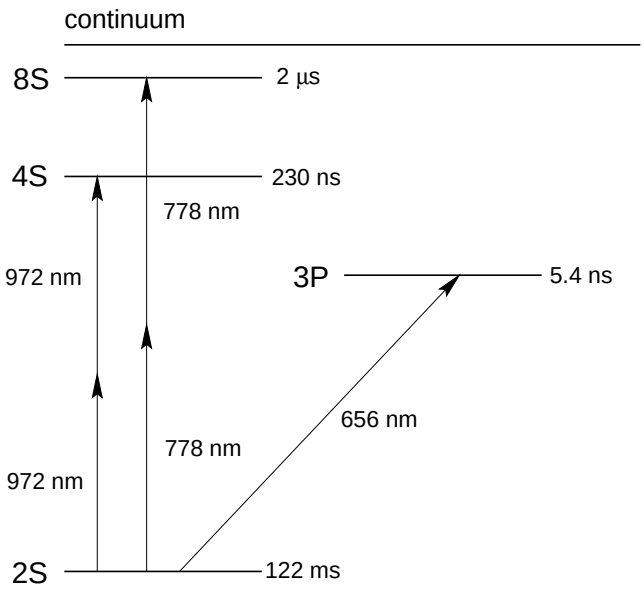

Figure 8: Energy level diagram showing transitions which will be excited in the hydrogen trap with stabilized diode lasers. The diode wavelengths and some natural lifetimes are indicated.

through the larger ground state cloud. In high density samples, however, the mean free path of a $2S$ atom between elastic collisions with $1S$ atoms becomes as short as 80 μm. At rf evaporation temperatures, the time it takes for the metastables to spread axially over the length (several centimeters) of the $1S$ cloud is much longer than the metastable lifetime. On the other hand, since the cloud has a thermal radius of only ~ 100 μm, an equilibrium distribution is quickly established in the radial direction. This combination of axial confinement by collisions and radial confinement by the magnetic field means that the static approximation is reasonable at high ground state densities.

The geometry factor G can be computed from the magnet currents and the known laser geometry, assuming a temperature simply related to the trap depth. The detection efficiency ϵ, however, is only known to lie between definite lower and upper bounds, separated by an order of magnitude. Taking the minimum possible detection efficiency, we find at 110 μK a lower bound for the two-body loss rate: $K_2 > 10^{-9}$ cm^3/s. After analysis of data constraining ϵ is complete, we expect a better determination of K_2. This is the first measurement of inelastic collisions for metastable H in the ultracold regime. R. C. Forrey, A. Dalgarno, and P. Froelich are presently calculating the relevant theoretical cross sections.

5 Outlook

Spectroscopy of Metastable H

The ability to produce trapped metastable H with lifetimes approaching the natural lifetime sets the stage for spectroscopy of the metastable sample. Fig. 8 shows the transitions which we plan to excite using stabilized diode lasers. The mirror inside our current trapping cell is dichroic, coated for both 243 nm and the 656 nm Balmer-α wavelength. This single photon transition can be used for absorption measurements of the $2S$ cloud, providing an additional tool for monitoring the $2S$ population. A Balmer-α laser is also potentially useful for photoassociation experiments. In a future apparatus, the 656 nm line could be used for imaging the sample.

With minor modifications to our cryogenic optics, we will be able to perform precision spectroscopy of $2S$-nS transitions. Our plan is first to excite the two-photon $2S$-$4S$ transition at 972 nm. The second harmonic of the 972 nm frequency differs by less than 5 GHz from the 486 nm source used for $1S$-$2S$ spectroscopy.

By offset locking the harmonic of a 972 nm diode to the $1S$-$2S$ frequency, the absolute frequency of the diode is determined with very high accuracy. To facilitate frequency metrology more generally, our group is acquiring a mode-locked femtosecond laser system [15]. The broad comb of frequencies generated by such a system will be used to measure $2S$-nS absolute frequencies and will permit the first precision measurement of the $1S$-$2S$ frequency using trapped H.

Trapping of Deuterium

Work is in progress to demonstrate magnetic trapping of deuterium (D). Deuterium is interesting to trap because it is a fermion, it has cold collision channels of theoretical interest, and trapping may allow precision measurements of isotope shifts. If D and H can be trapped simultaneously, then it may be possible to sympathetically cool deuterium to the Fermi-degenerate regime. On the other hand, since the elastic scattering length for H-D collisions is expected to be larger than for H-H collisions, the addition of D to a trapped H sample may allow for more efficient evaporative cooling of H.

Since the binding energy of D to the walls of our cell is much larger than for H, it is more difficult to load D into the magnetic trap. Methods for overcoming this obstacle are currently being explored. To unambiguously detect the presence of deuterium in our trap, our dye laser source can be tuned to search for the D $1S$-$2S$ transition.

Publications

Papers

T. J. Greytak, D. Kleppner, D. G. Fried, T. C. Killian, L. Willmann, D. Landhuis, and S. C. Moss, "Bose-Einstein condensation in atomic hydrogen", Physica B **280**, 20 (2000).

Thomas C. Killian, "$1S$-$2S$ Spectrum of a Hydrogen Bose-Einstein Condensate", Phys. Rev. A **61**, 033611 (2000).

Articles

Thomas J. Greytak and Daniel Kleppner, "Bose-Einstein condensation", in *McGraw-Hill Yearbook of Science and Technology 2001*, p. 64.

Lorenz Willmann and Daniel Kleppner, "Ultracold Hydrogen", in *Proceedings of the Conference* HII*, 2000*, edited by S. Karshenboim, *et al.* (in press).

Theses

Pan, Margaret, *Work on Diode Lasers for Spectroscopy of Atomic Hydrogen*, Senior Thesis, Department of Physics, MIT, 2001.

References

[1] T. J. Greytak, in *Bose-Einstein Condensation*, edited by A. Griffin, D. W. Snoke, and S. Stringari (Cambridge University Press, Cambridge, England, 1995).

[2] T. J. Greytak, D. Kleppner, D. G. Fried, T. C. Killian, L. Willmann, D. Landhuis, and S. C. Moss, Physica B **280**, 20 (2000).

[3] C. L. Cesar, D. G. Fried, T. C. Killian, A. D. Polcyn, J. C. Sandberg, I. A. Yu, T. J. Greytak, D. Kleppner, and J. M. Doyle, Phys. Rev. Lett. **77**, 255 (1996).

[4] T. C. Killian, D. G. Fried, L. Willmann, D. Landhuis, S. C. Moss, D. Kleppner, and T. J. Greytak, Phys. Rev. Lett **81**, 3807 (1998).

[5] H.-J. Miesner, D. M. Stamper-Kurn, M. R. Andrews, D. S. Durfee, S. Inouye, and W. Ketterle, Science **279**, 1005 (1998).

[6] M. J. Bijlsma, E. Zaremba, and H. T. C. Stoof, Phys. Rev. A **62**, 063609 (2000).

[7] S. Moss, E. Zaremba, H. T. C. Stoof, in preparation.

[8] M. Niering, R. Holzwarth, J. Reichert, P. Pokasov, T. Udem, M. Weitz, and T. W. Hänsch, Phys. Rev. Lett. **84**, 5496 (2000).

[9] C. Schwob, L. Jozefowski, B. de Beauvoir, L. Hilico, F. Nez, L. Julien, and F. Biraben, Phys. Rev. Lett. **82**, 4960 (1999).

[10] R. C. Forrey, R. Côté, A. Dalgarno, S. Jonsell, A. Saenz, and P. Froelich, Phys. Rev. Lett. **85**, 4245 (2000).

[11] M. Yasuda and F. Shimizu, Phys. Rev. Lett. **77**, 3090 (1996).

[12] A. Robert, O. Sirjean, A. Browaeys, J. Poupard, S. Nowak, D. Boiron, C. I. Westbrook, and A. Aspect, Science **292**, 461 (2001).

[13] K. S. Johnson, J. H. Thywissen, N. H. Dekker, K. K. Berggren, A. P. Chu, R. Younkin, and M. Prentiss, Science **280**, 1583 (1998).

[14] D. Landhuis, W. Joffrain, L. Matos, S. C. Moss, K. Vant, J. K. Steinberger, L. Willmann, T. J. Greytak, D. Kleppner, in preparation.

[15] T. Udem, J. Reichert, R. Holzwarth, and T. W. Hänsch, Optics Letters **24**, 881 (1999).